Tellus (1997), 49A, 100–107
Printed in UK – all rights reserved

TELLUS
ISSN 0280-6495

On the sensitivity of hail accretion rates in numerical modeling

By M. ĆURIĆ* and D. JANC, *Institute of Meteorology, University of Belgrade, P.O. Box 550, 11000 Belgrade, Yugoslavia*

(Manuscript received 20 June 1995; in final form 4 April 1996)

ABSTRACT

Numerical models of convective clouds with a bulk-water parameterization scheme extend the hail spectrum unrealistically to zero size. Since some of the microphysical characteristics of clouds depend critically on the hail accretional growth, it is desirable to see how the accretion rates may be improved by considering only hail sized particles, equal or greater than 0.5 cm in diameter. An equation for hail accretion rates which includes only hail particles larger than 0.5 cm is derived. Calculations show that the new hail accretion rates may differ from their earlier values by a factor of more than 3. The new equation for hail accretion rates is tested in a 1-D time-dependent model. The numerical results show that the modeled cloud with the new formula is more effective to produce the amount of rainfall and hail in shorter time than in previous case. The result is in fair agreement with observations.

1. Introduction

The hail acretion rates essentially contribute to the mass transfer between different precipitation elements in intense Cumulonimbus clouds. Therefore, their parameterizing in numerical models has received increased attention in recent years (Mizuno, 1990; Verlinde et al., 1990). Hail accretional growth is numerically treated by a collection equation. Most models with a bulk-water parameterization scheme use the approximate solutions to the integrand form of a stochastic collection equation introduced by Kessler (1969) and Wisner et al. (1972), like, for instance, Orville and Kopp (1977), Lin et al. (1983), Ćurić and Janc (1989, 1991, 1993) and Farley et al. (1994). These solutions are derived by integrating the corresponding equations over hail sizes from 0 to $+\infty$ (hereafter called the idealized hail spectrum) when hail follows two-moment exponential size distribution with one moment fixed. The hail size spectrum is treated rather loosely by taking into account the hail with size extension to zero, since the calculation of incomplete gamma functions is computationally expensive (Farley et al., 1989). However, the observed hail size spectrum is quite different. Therefore, the treatment of hail spectrum in existing models does not represent a real process.

In reality, a hailstone is a particle which has an equivalent sphere diameter of 0.5 cm or more (Pruppacher and Klett, 1978; Matson and Huggins, 1980; Bohm, 1989). Smaller sizes are attributed to different kinds of graupel (Bohm, 1989). On the other hand, graupel terminal velocities are mainly quite different compared to those for hail (Locatelli and Hobbs, 1974; Knight and Heymsfield, 1983; Heymsfield and Kajikawa, 1987; Murakami, 1990). Most hail models (e.g., Lin et al., 1983) assume the hail size distribution of exponential type found by Federer and Waldvogel (1975) adjusted for incloud conditions. Meanwhile, the graupel number concentrations are often

* Corresponding author.
e-mail: xpmfhn03@yubgss21.bg.ac.yu

of two orders of magnitude greater than those appropriate for large stones (Rutledge and Hobbs, 1984; Murakami, 1990; Randell et al., 1994). The inclusion of such a spectrum (a hailstone diameter of 0.5 cm or more), hereafter called the real hail spectrum, in modeled hail accretion rates may change their values compared to those derived with the idealized one.

We overcome the noted deficiencies of the idealized hail accretion rates (those with the idealized spectrum assumption) by considering the real hail spectrum. The accretion rates involve hail/rain, hail/snow and hail/cloud water (or cloud ice) interactions. The rate of hail accreting graupel is not considered according to Farley and Orville (1986) and Farley (1987). It is assumed that a graupel particle may attain the size comparable to that for a small hailstone by collecting water and other ice classes. The purpose of this study is to compare our hail accretion rates (those with the real spectrum assumption) and idealized ones. Finally, the formula for our accretion rates are tested in the 1-D forced time-dependent model of Ćurić and Janc (1993).

2. Hail terminal velocity

The knowledge of hail terminal velocities is important because they determine essentially the hail accretional growth. Idealized hail accretion rates (Lin et al., 1983; Farley et al., 1994) employ the hail terminal velocity introduced by Wisner et al. (1972):

$$U_{\mathrm{HD}} = \left(\frac{4 g \rho_{\mathrm{H}} D_{\mathrm{H}}}{3 C_{\mathrm{d}} \rho_{\mathrm{a}}} \right)^{1/2}, \tag{1}$$

(shown graphically in Fig. 1), where ρ_{H} and ρ_{a} are hail and air densities, whereas D_{H} is the diameter of a hailstone. Density of hail is assumed to be $\rho_{\mathrm{H}} = 900$ kg m^{-3}. Expression (1) follows the rigid sphere concept with a fixed drag coefficient ($C_{\mathrm{d}} = 0.6$) appropriate for the oblate spheroids as it was suggested by Macklin and Ludlam (1961). The other proposed hail terminal velocities (Roos and Carte, 1973; Matson and Huggins, 1980; Bohm, 1989; Mitchell, 1995), (all proportional to $D_{\mathrm{H}}^{1/2}$), underpredicts (1) by no more than 12%. Pruppacher and Klett (1978) proposed the expression for hail terminal velocity (proportional to $D_{\mathrm{H}}^{0.8}$) which overpredicts (1) only for the giant hailstones. These velocities are rarely employed in numerical modeling (Hu and He, 1988).

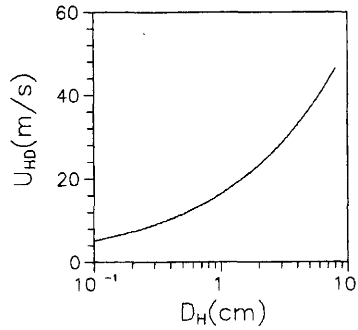

Fig. 1. Curve representing terminal velocity used versus hailstone diameter. It has been adjusted to an air density of 0.73 kg m^{-3}.

3. Hail accretion rates

Our hail accretion rates for two precipitation elements interacting may be determined from the continuous growth equation in the form:

$$P_{\mathrm{HX}} = |U_{\mathrm{X}} - U_{\mathrm{H}}| \int_{0}^{+\infty} \int_{D_{\mathrm{H}}^{*}}^{+\infty} \overline{E_{\mathrm{HX}}} \frac{\pi^2}{24} \times (D_{\mathrm{X}} + D_{\mathrm{H}})^2 N_{\mathrm{XD}} D_{\mathrm{X}}^3 \frac{\rho_{\mathrm{X}}}{\rho_{\mathrm{a}}} N_{\mathrm{HD}} \, \mathrm{d}D_{\mathrm{X}} \, \mathrm{d}D_{\mathrm{H}}, \tag{2}$$

where $\overline{E_{HX}}$ is the collection efficiency of hail for particle-X. P_{HX} is the total mixing ratio increase rate of hail due to the accretion of the X particles. The subscript X refers to rain (R) or snow (S), respectively; D_{X} is a diameter of particle X; $D_{\mathrm{H}}^{*} = 0.5$ cm; N_{XD} and N_{HD} are spectral densities of diameters D_{X} and D_{H}, while ρ_{R} and ρ_{S} are densities of water and snow. Terminal velocities U_{X} and U_{H} represent the mass-weighted particle velocities for particle-X and hail respectively. That for hail is following the Srivastava (1967) method:

$$U_{\mathrm{H}} = \frac{\int_{D_{\mathrm{H}}^{*}}^{+\infty} U_{\mathrm{HD}} Q_{\mathrm{HD}} \, \mathrm{d}D_{\mathrm{H}}}{\int_{D_{\mathrm{H}}^{*}}^{+\infty} Q_{\mathrm{HD}} \, \mathrm{d}H_{\mathrm{H}}}. \tag{3}$$

In (3), Q_{HD} is the mixing ratio of hail of diameter D_{H}. With regard to possible application in numerical modeling, we include into our hail accretion rates the most widely used hail terminal velocity (eq. (1)). Then, eq. (3) becomes

$$U_H = \frac{\Gamma(4.5)}{6(\lambda_H)^{0.5}} \frac{1-\alpha_1}{1-\alpha_2} \left(\frac{4g\rho_H}{3C_d\rho_a}\right)^{1/2}. \tag{4}$$

The parameters α_1 and α_2 that include the incomplete gamma functions (Abramowitz and Stegun, 1970) are defined as follows

$$\alpha_1 = \frac{\Gamma(4.5; \lambda_H D_H^*)}{\Gamma(4.5)}; \qquad \alpha_2 = \frac{\Gamma(4; \lambda_H D_H^*)}{\Gamma(4)} \tag{5}$$

For real hail spectrum, the slope parameter λ_H for the hail size distribution is obtained in the form:

$$\lambda_H = \lambda_{H0} f^{0.25}; \qquad \lambda_{H0} = \left(\frac{\pi \rho_H N_{0H}}{\rho_a Q_H}\right)^{0.25}, \tag{6}$$

where λ_{H0} is the slope parameters as used in previous hail models (Lin et al., 1983; Farley et al., 1994), while f is a coefficient defined as follows:

$$f = 1 - \frac{\Gamma(4; \lambda_H D_H^*)}{\Gamma(4)}. \tag{7}$$

As noted from eq. (6), the slope parameter so far used (λ_{H0}) is now multiplied by a factor of $f^{0.25}$.

In eq. (6), N_{0H} is the intercept value in hail size distribution taken to be $4 \times 10^4\ \mathrm{m}^4$ according to Lin et al. (1983), while $\rho_a = 0.73\ \mathrm{kg\,m^{-3}}$ in our calculations.

Our mass-weighted particle velocity defined by eqs. (4)–(7) and idealized ones (calculated from eq. (4) when $D_H^* = 0$) versus hail mixing ratio (ranged from 5×10^{-4} to $5 \times 10^{-3}\ \mathrm{kg\,kg^{-1}}$) are shown graphically in Fig. 2. As can be seen, the velocities we compute are considerably higher than what was obtained for the idealized spectrum, especially for lower hail mixing ratios. The difference attains a maximum of $3.4\ \mathrm{m\,s^{-1}}$ for $Q_H = 5 \times 10^{-4}\ \mathrm{kg\,kg^{-1}}$. This is induced primarily by the coefficient f (eqs. (6) and (7)).

Eq. (7) clearly shows the size range of the coefficient f. Its maximum value ($f = 1$) is attained for idealized hail spectrum ($D_H^* = 0$). In general, the real hail spectrum (eqs. (6) and (7)) induces a lower slope parameter compared to an idealized case, needed to enable the same mixing ratio. Consequently, this implies more large stones compared to the idealized hail spectrum. The coefficient f versus hail mixing ratios is shown in Fig. 3. Its maximum value ($f = 0.7$) is reached for $Q_H = 5 \times 10^{-3}\ \mathrm{kg\,kg^{-1}}$ and $\rho_a = 1\ \mathrm{kg\,m^{-3}}$. It is determined by solving the corresponding transcendental equation with a relative error less than 0.1%.

Our accretion rates when hail accretes monodisperse size distributed cloud water (or cloud ice) may be derived under the assumption that their sizes and terminal velocities can be disregarded compared to those for hail. Thus, it becomes:

$$P_{HY} = \int_{D_H^*}^{+\infty} \overline{E_{HY}} \frac{\pi}{4} D_H^2 U_{HD} N_{HD} Q_Y \, dD_H, \tag{8}$$

where $\overline{E_{HY}}$ is the collection efficiency of hail for particles-Y; Y refers to cloud water (C) or cloud ice (I), while Q_Y is the corresponding mixing ratio.

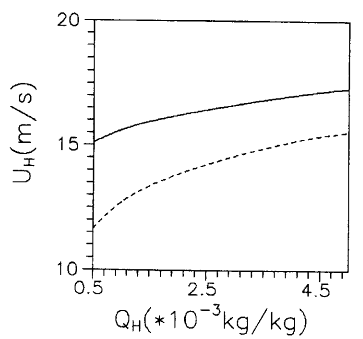

Fig. 2. Mass-weighted mean particle velocity plotted against hail mixing ratio. Our and idealized ones are designated by solid and dashed lines, respectively.

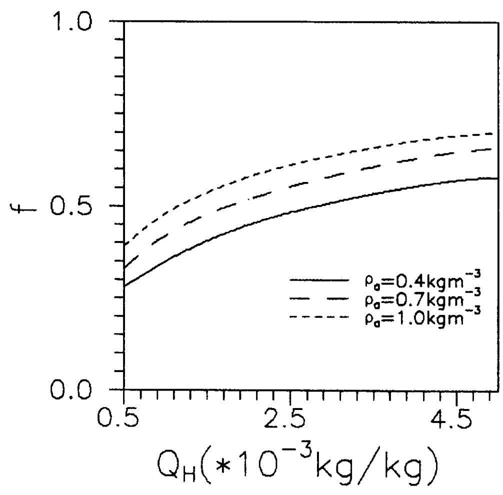

Fig. 3. Coefficient f versus hail mixing ratio for different air densities.

Our accretion rates (2) and (8) use the mass-weighted particle velocity (4) and the slope parameter (6). They are presented in Section 8.

4. Comparison of hail accretion rates

This section reports the results of comparisons which are made between our and idealized hail accretion rates. The comparisons are presented as:

$$k = \log_{10}\left(\frac{P_{HZ1}}{P_{HZ2}}\right), \tag{9}$$

where the subscript Z refers to rain (R), snow (S) and cloud water (C). Our accretion rate P_{HZ1} is compared to the idealized value P_{HZ2}. Positive k values indicate that our hail accretion rate overestimates the idealized value, while negative values indicate underestimation.

Two-dimensional plot diagrams (Figs. 5, 6) use the modified values $Q_{\Omega T}$ instead of original mixing ratios Q_Ω, which ranged from 5×10^{-4} to 5×10^{-3} kg kg^{-1} for rain and hail, or from 10^{-7} kg kg^{-1} to 5×10^{-3} kg kg^{-1} for snow. The subscript Ω refers to rain (R), hail (H) and snow (S), respectively. The relationship between both values are:

$$Q_{\Omega T} = \log_{10} Q_\Omega + 7. \tag{10}$$

Fig. 4 shows our and idealized hail accretion rates for certain values of hail mixing ratio. The mixing ratio of the class of particle being accreted

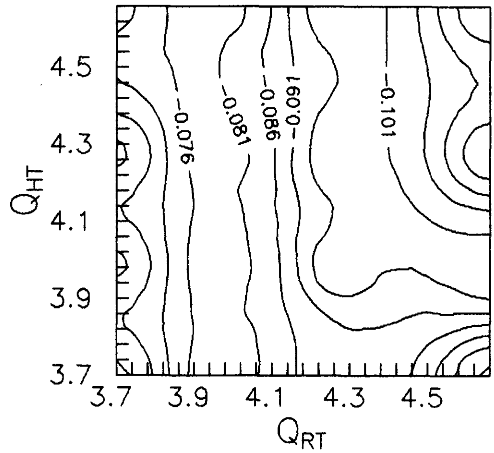

Fig. 5. Ratio k, when hail accretes rain, for various hail and rain mixing ratios. The modified values of corresponding mixing ratios instead of original ones are used.

is taken to be 10^{-3} kg kg^{-1}. Compared to the idealized one, the real hail spectrum contains more large hailstones providing greater mass-weighted particle velocities and smaller hail number concentration. This leads to reduced hail/rain (or snow) accretion rate, (Fig. 4a-b). In contrast to hail/rain (or snow) case, the accretion rate when hail accretes cloud water is now enhanced (Fig. 4c).

Smaller number concentrations of hailstones in real spectrum compared to idealized one weakens the effectiveness of collisions between hail and large drops. Therefore, the new accretion rate of

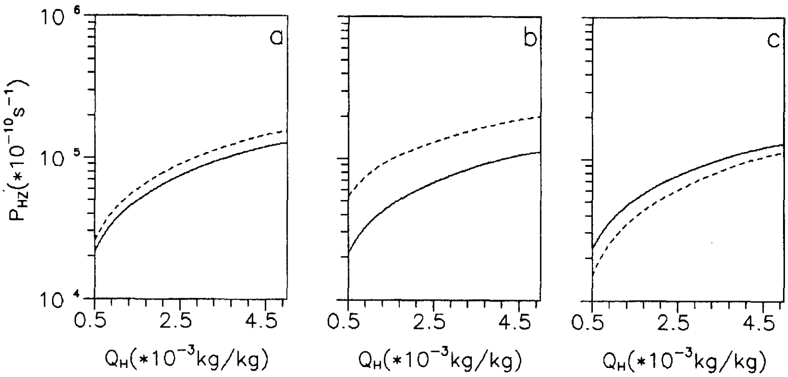

Fig. 4. Accretion rate, $P_{HZ}(\times 10^{-10}\,s^{-1})$, versus hail mixing ratio when hail interacts with: (a) rain; (b) snow and (c) cloud water, for $Q_Z = 10^{-3}$ kg kg^{-1}. Our and idealized accretion rates are designated by solid and dashed lines, respectively.

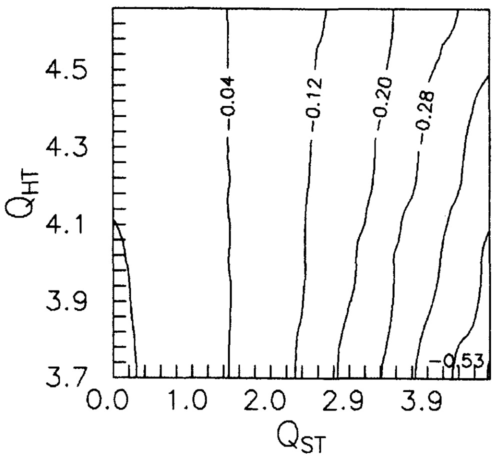

Fig. 6. As in Fig. 5 but when hail accretes snow.

rain by hail is reduced by 13–24% ($k = -0.06$ and -0.119), as can be seen in Fig. 5. The minimum k-value is found out for large rain and hail mixing ratios.

Fig. 6 demonstrates k-ratios for the accretion rate when hail accretes snow plotted against modified hail and snow mixing ratios. Our accretion rates are reduced by a factor of 3.4 ($k = -0.53$). In contrast to hail/rain case, the minimum k-ratio value is displaced towards the lowest hail mixing ratio. This is attributed to low density snow flakes providing lower number concentration compared to that for rain.

Fig. 7 clearly shows that our accretion rates when hail accretes cloud water (or cloud ice) always overpredict corresponding idealized values.

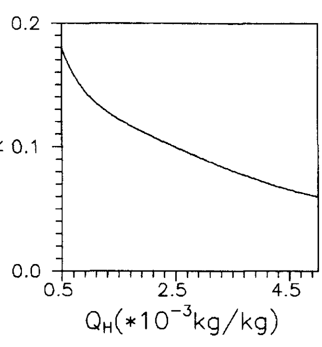

Fig. 7. Ratio (k) between our and idealized accretion rates when hail accretes cloud water versus hail mixing ratio.

They are enhanced by 15–51%. More large hailstones in real hail spectrum compared to idealized case essentially determine the effectiveness of the collection of small droplets.

Calculations with the other expressions (results not shown here) for hail terminal velocity (all proportionate to D_H^b) indicate that the k-ratios are very sensitive to an exponent (b). For instance, Pruppacher and Klett (1978) expression with $b = 0.8$ instead of (1) significantly changes the k-ratios. Then, our accretion rate when hail accretes the rain is enhanced by a factor of 77.6.

5. Hail accretion rates in a numerical model

Since some of the microphysical characteristics of a cloud depend critically on the accretion, it is instructive to see how these constituents are induced by accretion. The change of cloud microphysics involved by eqs. (2) and (8) have been examined via a numerical model. The model applied is a 1-D time-dependent model. The version used here was proposed by Ćurić and Janc (1988). It was further modified, including new ways of representing entrainment, forced lifting and pressure perturbation (Ćurić and Janc, 1993). It combines dynamical equation with water continuity equations that include ice phase microphysical processes.

Fig. 8 shows the time-height cross section of hail (Q_H), rain (Q_R) and cloud water (Q_C) mixing ratios. The influence of the difference in the hail size domain (Figs. 8 to the left, case (a), refer to idealized hail spectrum; those to the right, case (b), are for real one) is shown for a simulated storm based on the 23 June 1985 sounding at Belgrade. It can be seen that hailstones are produced earlier in case (a) than in (b) in the middle part of a cloud, as clearly shown in contour of 0.2×10^{-3} kg kg^{-3}. Fig. 8 (left) shows that Q_H continues to increase with time at all levels of a cloud until 14 min when its peak value of 5×10^{-3} kg kg^{-1} appears at the level of 5 km.

The peak value of $Q_H = 4.6 \times 10^{-3}$ kg kg^{-1} appears at the level of 7 km at 15 min in case (b), and its extension to lower levels is faster than in case (a) due to the higher values of the mass-weighted particle velocity of hail (see Fig. 2). After 15 min, there are some different evolution of Q_H for cases (a) and (b). It is to be noted that in case

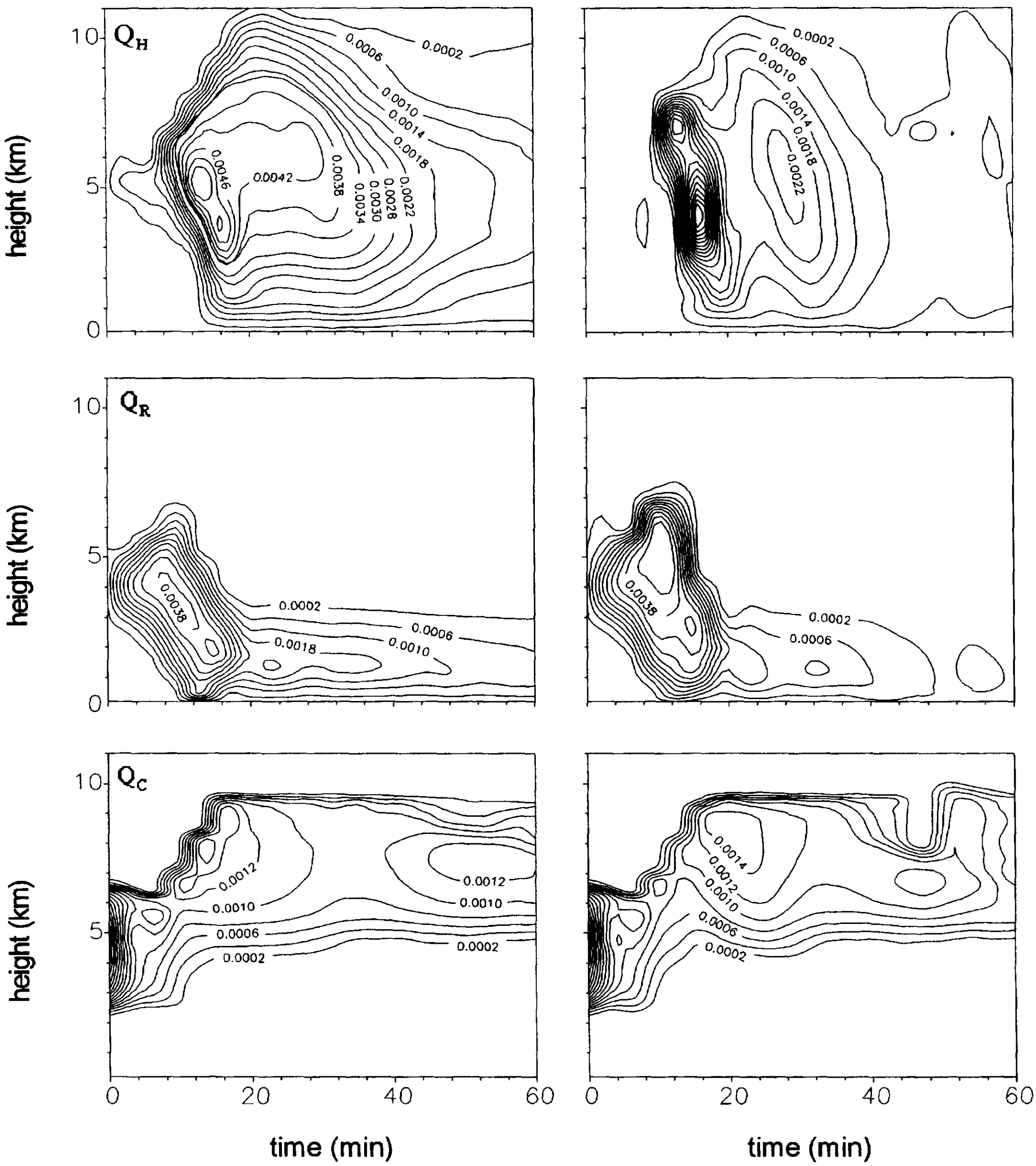

Fig. 8. Time-height cross-sections of hail (Q_H), rain (Q_R) and cloud water (Q_C) mixing ratios for idealized (to the left) and our (to the right) hail accretion rates. Height (km) above ground level.

(a), in which many small hailstones are assumed to exist, it tends to decrease with time more slowly than in case (b).

The rearrangements with time of rain and cloud water are also depicted in Fig. 8. It can be seen that raindrops are produced earlier than hail. The maximum of Q_R is reached at the higher level in case (b) than in case (a). In both cases drops with $Q_R = 0.2 \times 10^{-3}$ kg kg^{-1} reach the ground nearly at the same time. Later, hail through the accretion removes rain water from the cloud, leading to a faster decrease with time of Q_R in case (b) than in case (a). Therefore, the modeled cloud with the new formula for hail accretion rates (eqs. (2) and (8)) would be more effective to produce the amount of rainfall and hail in reasonably shorter time than previously. This result is in fair agreement with observation. Thus, the need for a more complete description of accretion was justified.

6. Conclusions

Our hail accretion rates treat the hail spectrum by considering only hail sized particles, and not extending it unrealistically to zero size. Consequently, significant differences of their values compared to idealized accretion rates are found.

Our accretion rates are reduced compared to idealized ones when hail collides with raindrops and snow. In contrast, they are enhanced when hail/cloud water (ice) interaction is considered. Our hail accretion rates differ from corresponding idealized values by a factor of 3.4.

In order to show how our accretion equation induces a change of some microphysical characteristics of a cloud, additional numerical experiments were conducted. They show that the modeled cloud with the new formula is more effective in removing the rain and hail in shorter time than in idealized case. The results shown here offer an example that a change in hail spectrum domain leads to a profound effect on the simulated cloud life. Therefore, the need for a more complete description of the hail accretion rates is still actual.

7. Acknowledgements

This research was partly supported by the Science Association of Serbia. Two anonymous reviewers have made many suggestions in the reviewing process that increased the completeness and clarity of the paper. These contributions are appreciated.

8. Appendix

New hail accretion rates

Our accretion rate at which a hailstone collides with raindrops or snow is:

$$P_{\mathrm{HX}} = \frac{\pi^2}{24} \overline{E_{\mathrm{HX}}} \frac{\rho_{\mathrm{X}}}{\rho_{\mathrm{a}}} N_{0\mathrm{X}} N_{0\mathrm{H}} |U_{\mathrm{X}} - U_{\mathrm{H}}| \times \left[\frac{\Gamma(6)\Gamma(1)(1-\beta_1)}{\lambda_{\mathrm{R}}^6 \lambda_{\mathrm{H}}} + \frac{\Gamma(5)\Gamma(2)(1-\beta_2)}{\lambda_{\mathrm{R}}^5 \lambda_{\mathrm{H}}^2} + \frac{\Gamma(4)\Gamma(3)(1-\beta_3)}{\lambda_{\mathrm{R}}^4 \lambda_{\mathrm{H}}^3} \right] \tag{11}$$

where

$$\beta_1 = \Gamma(1; \lambda_{\mathrm{H}} D_{\mathrm{H}}^*), \qquad \beta_2 = \Gamma(2; \lambda_{\mathrm{H}} D_{\mathrm{H}}^*), \qquad \beta_3 = 0.5 \times \Gamma(3; \lambda_{\mathrm{H}} D_{\mathrm{H}}^*). \tag{12}$$

In (11) $N_{0\mathrm{R}}$ and $N_{0\mathrm{S}}$ are the intercept values in rain and snow size distributions supposed to be fixed with respective values of $N_{0\mathrm{R}} = 8 \times 10^6\ \mathrm{m}^{-4}$ and $N_{0\mathrm{S}} = 3 \times 10^6\ \mathrm{m}^{-4}$; $\rho_{\mathrm{R}} = 10^3\ \mathrm{kg\ m}^{-3}$; $\rho_{\mathrm{S}} = 10^2\ \mathrm{kg\ m}^{-3}$; $\overline{E_{\mathrm{HR}}} = 1$, while $\overline{E_{\mathrm{HS}}}$ is dependent on temperature for cold regions of a cloud. If the temperature is warmer than 0°C, it is assumed to be 1. Corresponding mass-weighted particle velocities for rain or snow (U_{X}) are:

$$U_{\mathrm{X}} = \frac{a_{\mathrm{X}} \Gamma(4+i)}{6 \lambda_{\mathrm{X}}^i} \left(\frac{\rho_0}{\rho_{\mathrm{a}}} \right)^{1/2}, \tag{13}$$

where λ_{X} is the slope parameter for rain (λ_{R}) or snow (λ_{S}) size distribution; $a_{\mathrm{R}} = 842\ \mathrm{m}^{0.2}\ \mathrm{s}^{-1}$, $a_{\mathrm{S}} = 4.84\ \mathrm{m}^{0.75}\ \mathrm{s}^{-1}$, $\rho_0 = 1.2 \times 10^3\ \mathrm{kg\ m}^{-3}$, while i takes values of 0.8 for rain and 0.25 for snow, respectively. All values of the parameters used are taken from Lin et al. (1983).

Our rate at which hail collides with cloud droplets (or cloud ice), for the monodisperse size distributed cloud droplets (cloud ice), may be written in the form:

$$P_{\mathrm{HY}} = \frac{\pi \overline{E_{\mathrm{HY}}} N_{0\mathrm{H}} \Gamma(3.5)(1-\delta) Q_{\mathrm{Y}}}{4 \lambda_{\mathrm{H}}^{3.5}} \left(\frac{4 g \rho_{\mathrm{H}}}{3 C_{\mathrm{d}} \rho_{\mathrm{a}}} \right)^{1/2}, \tag{14}$$

where

$$\delta = \frac{\Gamma(3.5; \lambda_{\mathrm{H}} D_{\mathrm{H}}^*)}{\Gamma(3.5)}. \tag{15}$$

In (14), $\overline{E_{\mathrm{HY}}}$ are assumed equal to 1.0 for cloud water and ice, but only 0.1 for hail collecting cloud ice in the dry growth regime.

REFERENCES

Abramowitz, M. and Stegun, I. A. 1970. *Handbook of mathematical functions with formulas, graphs, and mathematical tables.* Dover, 364 pp.

Bohm, H. P. 1989. A general equation for the terminal fall speed of solid hydrometers. *J. Atmos. Sci.* **46**, 2419–2427.

Ćurić, M. and Janc, D. 1988. A forced 1-D convective cloud model. *Meteorol. Atmos. Phys.* **39**, 51–62.

Ćurić, M. and Janc, D. 1989. Dynamic entrainment rate influence on products of a one-dimensional cumulonimbus model. *Atmos. Res.* **24**, 305–323.

Ćurić, M. and Janc, D. 1991. Graupel growth and trajectories in a shallow Cb cloud determined by a forced 1-D model. *Atmosphere-Ocean* **29**, 462–478.

Ćurić, M. and Janc, D. 1993. Predictive capabilities of a one-dimensional convective cloud model with forced lifting and a new entrainment formulation. *J. Appl. Meteor.* **32**, 1733–1740.

Farley, R. D. 1987. Numerical modeling of hailstorms and hailstone growth. Part II: The role of low-density riming growth in hail production. *J. Climate Appl. Meteor.* **26**, 234–254.

Farley, R. D. and Orville, H. D. 1986. Numerical modeling of hailstorms and hailstone growth. Part I: Preliminary model verification and sensitivity tests. *J. Climate Appl. Meteor.* **25**, 2014–2035.

Farley, R. D., Price, P. E., Orville, H. D. and Hirsch, J. H. 1989. On the numerical simulation of graupel/hail initiation via the riming of snow in bulk water microphysical cloud models. *J. Climate Appl. Meteor.* **28**, 1128–1131.

Farley, R. D., Nguyen, P. and Orville, H. D. 1994. Numerical simulation of cloud seeding using a three-dimensional cloud model. *J. Wea. Mod.* **26**, 113–124.

Federer, B. and Waldvogel, A. 1975. Hail and raindrop size distributions from a Swiss multicell storm. *J. Appl. Meteor.* **14**, 91–97.

Heymsfield, A. and Kajikawa, M. 1987. An improved approach to calculating terminal velocities of plate-like crystals and graupel. *J. Atmos. Sci.* **44**, 1088–1099.

Hu, Z. and He, G. 1988. Numerical simulation of microphysical processes in cumulonimbus — Part I: Microphysical model. *Acta Meteorological Sinica* **2**, 471–489.

Kessler, E. 1969. On the distribution and continuity of water substance in atmospheric circulations. *Meteor. Monogr.* no. **32**, Amer. Meteor. Soc., 84 pp.

Knight, N. C. and Heymsfield, A. J. 1983. Measurement and interpretation of hailstone density and terminal velocity. *J. Atmos. Sci.* **40**, 1510–1516.

Lin, Y.-L., Farley, R. D. and Orville, H. D. 1983. Bulk parameterization of the snow field in a cloud model. *J. Atmos. Sci.* **22**, 1065–1089.

Locatelli, J. D. and Hobbs, P. V. 1974. Fallspeeds and masses of solid precipitation particles. *J. Geophys. Res.* **79**, 2185–2197.

Macklin, W. C. and Ludlam, F. H. 1961. The fall speeds of hailstones. *Quart. J. Roy. Meteor. Soc.* **87**, 72–81.

Matson, R. J. and Huggins, A. W. 1980. The direct measurement of the sizes, shapes and kinematics of falling hailstones. *J. Atmos. Sci.* **37**, 1107–1125.

Mitchell, D. L. 1995. A simple expression for accurately calculating precipitation fallspeeds for any particle type. *Proceedings from AMS Conference on Cloud Physics*, 15–20 January, Dallas, 46–49.

Mizuno, H. 1990. Parameterization of the accretion process between different precipitation elements. *J. Meteor. Soc. Japan* **57**, 273–281.

Murakami, M. 1990. Numerical modeling of dynamical and microphysical evolution of an isolated convective cloud. The 19 July 1981 CCOPE cloud. *J. Meteor. Soc. Japan* **68**, 107–128.

Orville, H. D. and Kopp, F. J. 1977. Numerical simulation of the life history of a hailstorm. *J. Atmos. Sci.* **34**, 1596–1618.

Pruppacher, H. R. and Klett, J. D. 1978. *Microphysics of clouds and precipitation.* D. Reidel, 714 pp.

Randell, S. C., Rutledge, S. A., Farley, R. D. and Helsdon, J. H., Jr. 1994. A modeling study on the early electrical development of tropical convection: continental and oceanic (monsoon) storms. *Mon. Wea. Rev.* **122**, 1852–1877.

Roos, D. Van der S. and Carte, A. E. 1973. The falling behaviour of oblate and spiky hailstones. *J. Rech. Atmos.* **7**, 39–52.

Rutledge, S. A. and Hobbs, P. V. 1984. The mesoscale and microscale structure and organization of clouds and precipitation in midlatitude cyclones. XII: A diagnostic modeling study of precipitation development in narrow cold-frontal rainbands. *J. Atmos. Sci.* **41**, 2949–2972.

Srivastava, R. C. 1967. A study of the effects of precipitation on cumulus dynamics. *J. Atmos. Sci.* **24**, 36–45.

Verlinde, J., Flatau, P. J. and Cotton, W. R. 1990. Analytical solutions to the collection growth equation: comparison with approximate methods and applications to cloud microphysics parameterization schemes. *J. Atmos. Sci.* **47**, 2871–2880.

Wisner, C., Orville, H. D. and Myers, C. 1972. A numerical model of a hail-bearing cloud. *J. Atmos. Sci.* **29**, 1160–1181.